Available online at www.sciencedirect.com
SCIENCE DIRECT®
ELSEVIER
Journal of Magnetism and Magnetic Materials 278 (2004) 57–67
Journal of magnetism and magnetic materials
www.elsevier.com/locate/jmmm

Influence of Mo-doping on the magnetic properties of V_2O_3

C. Tenailleau[a], E. Suard[b], J. Rodriguez-Carvajal[c], P. Lacorre[a,*]

[a] *Laboratoire des Fluorures, UMR CNRS 6010, Université du Maine, Avenue Olivier-Messiaen, F-72085 Le Mans cedex 9, France*
[b] *Institut Laue Langevin, Avenue des Martyrs, B.P. 156, F-38042 Grenoble cedex 9, France*
[c] *Laboratoire Léon Brillouin (CEA-CNRS), Centre d'Etudes de Saclay, F-91191 Gif-sur-Yvette cedex, France*

Received 8 September 2003; received in revised form 17 November 2003

Abstract

The magnetic study of new Mo-doped vanadium sesquioxides $(V_{1-x}Mo_x)_{2-\delta}O_3$ revealed two unexpected behaviours. On the one hand, the measured effective magnetic moment in the paramagnetic state at room temperature exhibits a peculiar variation against Mo-doping: first it increases for the lower doping rates ($x \leqslant 5\%$ with a metal/insulator transition), then decreases for purely metallic compositions ($x > 5\%$). This could be explained by the existence of a spin–orbit coupling between cations. On the other hand, a very weak ferromagnetic component has been evidenced in addition to the mainly antiferromagnetic behaviour. This ferromagnetism is correlated to the partial oxidation of the samples in air at room temperature. The magnetic structure of Mo-doped compounds is similar to that of V_2O_3, but with a small rotation of the magnetic moment as a function of doping. In contrast with the effect of titanium doping, no magnetic ordering has been observed at low temperature for the highly Mo-doped samples ($x > 5\%$), which remain metallic over the whole thermal range.

PACS: 75.20.−g; 75.25.+z; 75.30.Cr; 75.60.Ej; 71.30.+h

Keywords: Mo-doped vanadium sesquioxide; Oxidation in air; Neutron diffraction; Magnetic behaviour; Ferromagnetic component; Spin–orbit coupling

1. Introduction

Vanadium sesquioxide V_2O_3 is thought to be a typical example of an oxide with a Mott metal–insulator transition [1–3]. At the first-order transition at 160 K, there is a symmetry change from rhombohedral at high temperature to monoclinic at low temperature.

In the $160\,K \leqslant T \leqslant 400\,K$ range the metallic phase shows a regular paramagnetic behaviour, instead of the usual Pauli's paramagnetism expected for a metal. The χ susceptibility follows a Curie–Weiss law: $\chi = C/(T-\theta)$ with $C = 0.657$ (emu/mole/K) and $\theta = -600\,K$. The C value is reasonable for a V^{3+} ion, i.e. in the $3d^2$ electronic state. The effective magnetic moment per vanadium atom is equal to $2.37\,\mu_B$ as compared to the theoretical value of $2.83\,\mu_B$ [4,5].

*Corresponding author. Tel.: +33-2-4383-2643; fax: +33-2-4383-3506.
E-mail address: philippe.lacorre@univ-lemans.fr (P. Lacorre).

0304-8853/$ - see front matter © 2003 Elsevier B.V. All rights reserved.
doi:10.1016/j.jmmm.2003.11.373

Simultaneous to the electrical and structural changes, a magnetic ordering occurs abruptly in the monoclinic phase. The antiferromagnetism in V_2O_3 at low temperature was evidenced by R.M. Moon through neutron spin-flip diffraction [6,7].

The magnetic structure of V_2O_3 is peculiar. The magnetic moment per vanadium atom is $1.20\,\mu_B$ instead of the $2\,\mu_B$ expected for a $3d^2$ cation ($S = 1$). The moments are aligned with each other within the $(0,1,0)_m$ monoclinic planes, with an antiparallel ordering from one plane to the next one. The magnetic moments form an angle close to 20° with the a_m monoclinic axis. Within the pseudo-hexagonal reference set, each moment is perpendicular to the a_h axis, forming an angle of 71° with the c_h axis [8].

We have recently shown the existence of a new family of doped vanadium sesquioxide $(V_{1-x}Mo_x)_{2-\delta}O_3$ and studied its properties [9]. The synthesis conditions and structural characteristics of this family were reported elsewhere [10–12]. EPR spectroscopy measurements [13] have evidenced two correlated effects: weak vanadium oxidation and ferromagnetism in samples exposed to air at ambient temperature. Both effects disappear when the samples are annealed in dilute hydrogen.

In the current paper we present the magnetic properties of $(V_{1-x}Mo_x)_{2-\delta}O_3$. After the experimental section, magnetic susceptibility measurements will be reported and analysed in Section 3. Then Section 4 will be devoted to the magnetisation properties study of oxidised and reduced samples, in fields up to 7 T at various temperatures. The effect of temperature and Mo doping on the vanadium sesquioxide magnetic structure, as determined from neutron diffraction patterns, will be presented in Section 5, before a summary and conclusion in Section 6.

2. Experimental

The $(V_{1-x}Mo_x)_{2-\delta}O_3$ samples preparation was reported in a previous article [10]. Small amount of powder samples were prepared from stoichiometric mixtures of V_2O_3 and MoO_2 heated in a high-frequency induction furnace under vacuum (about 10^{-6} mbar) at 870°C. After intermediate grindings, this process was repeated several times for several samples in order to get several grams of pure materials.

A Quantum Design 6000 Model PPMS (Physical Properties Measurement System) instrument of has been used for AC and DC magnetic measurements in the (2–300 K) range with a magnetic field varying up to 7 T. The sample (typically 250 mg of powder), enclosed in a diamagnetic pharmaceutical capsule, is placed at the extremity of a diamagnetic straw. The latter can move longitudinally and parallel to the magnetic field. The magnitude, frequency and acquisition time of the small alternative magnetic field used during the AC measurements were 14 Oe, 1234 Hz and 5 s, respectively.

Neutron diffraction patterns were recorded on Debye-Scherrer diffractometers D2B (ILL, Grenoble, $\lambda = 1.5941$ Å) and 3T2 (LLB, Saclay, $\lambda = 1.2252$ Å) for magnetic structure determination at 10 K, and D1B (ILL, Grenoble, $\lambda = 2.520$ Å) and G4.1 (LLB, Saclay, $\lambda = 2.427$ Å) for thermal evolution.

3. Magnetic susceptibility

None of the AC susceptibility measurements done in the conditions defined previously shows any imaginary contribution. For a given sample, the AC susceptibility curves are perfectly superimposed, in the high temperature phase, for a magnetic field higher than 0.5 T (see Fig. 1 for $x = 5\%$). At lower fields, the curves are translated to slightly higher values, but the slope is always identical much above the transition temperature. As a consequence, the molar Curie constant is the same irrespective of the constant field applied to the sample.

Fig. 2 shows the thermal evolutions of the inverse molar magnetic susceptibility $1/\chi_m$ for samples $x = 0\%$, 2%, 3%, 4%, 5%, 7%, 10% and 20%, under a field of 7 T (after subtraction of the diamagnetic components).

For $x \leqslant 5\%$ there is an abrupt increase of the susceptibility while magnetic ordering occurs. The higher the amount of molybdenum in the sample,

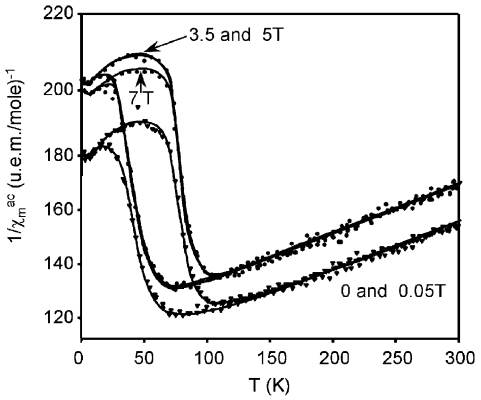

Fig. 1. Temperature dependence of the reciprocal AC susceptibility of $(V0_{.95}Mo_{0.05})_{2-\delta}O_3$ under 0, 0.05, 3.5, 5 and 7 T.

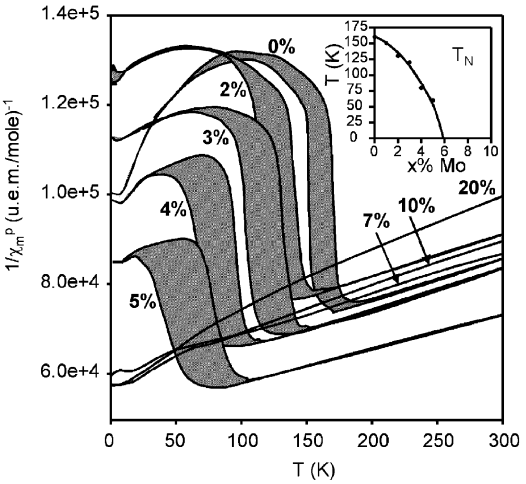

Fig. 2. Temperature dependence of the reciprocal paramagnetic molar susceptibility of $(V_{1-x}Mo_x)_{2-\delta}O_3$ with $x = 0\%$, 2%, 3%, 4%, 5%, 7%, 10%, and 20%. In inset: variation with x of the magnetic transition temperature (middle of the hysteresis cycle).

the lower the magnetic transition temperature is. This temperature is very close to the metal/insulator and structural transition temperatures. For the samples which exhibit a magnetic transition the hysteresis cycle appears to enlarge with the substitution of molybdenum in the samples. This observation is in agreement with a previous study on the thermal evolution of the relative amount of rhombohedral phase for different Mo-doping rates [12]. The nucleation of the minority phase is slower when the transition temperature is lower. So the first-order transition shows an increase of the hysteresis with the Mo-doping rate. No abrupt magnetic susceptibility variation is observed when $x = 10\%$ and 20%, but a small variation in the slope is observed around 75 K.

At room temperature χ_m increases with x up to $x = 5\%$ and decreases for higher Mo-doping rates. A Curie–Weiss law being observed, the C_m molar Curie constant can be calculated from the thermal evolution of the paramagnetic part of $1/\chi_m$. The Curie constant, and therefore the effective magnetic moment, do not exhibit any monotonous variation with the Mo-doping rate. Two domains can be defined (Fig. 3):

- for $0 < x \leqslant 5\%$, typically the samples showing a metal/insulator transition at low temperature, the effective magnetic moment increases with the Mo-doping rate;
- for higher Mo-doping rates ($x > 5\%$), in compounds remaining metallic over the whole thermal range, the effective magnetic moment decreases with Mo substitution.

The effective moment measured in V_2O_3 (2.58 μ_B) is in good agreement with the values published in the literature for this compound [4,5]

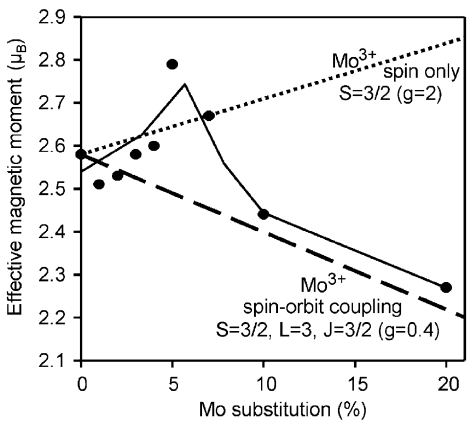

Fig. 3. Variation with x of the effective magnetic moment of $(V_{1-x}Mo_x)_{2-\delta}O_3$, and comparison with the theoretical variation assuming spin-only (dotted line) and spin–orbit (dashed line) for Mo^{3+} ions (see text).

and for a $3d^2$ cation [14]. Its value increases with low Mo-doping rates. This is coherent with the progressive substitution by trivalent molybdenum ($4d^3$), which has one more unpaired electron than trivalent vanadium. However, the decrease of the observed magnetic moment with higher doping rates appears more problematic. It corresponds to a decrease of the number of unpaired electrons in the system, which might be due for instance to an oxidation of vanadium or molybdenum. In order to explain the reduction of the observed moment in the sample with $x = 20\%$, an amount of V^{4+} between 70% and 100% (depending on the amount of tetravalent molybdenum) would be necessary, which is definitively not realistic. As a matter of fact EPR measurements [13] showed that the quantity of V^{4+} is very low in all our samples ($<0.03\%$), and structural studies revealed that molybdenum is in a trivalent state for all compositions [11].

Another way to justify a reduction of the moment would be to consider the existence of a spin–orbit coupling. Depending on the electronic shells occupation, the spin–orbit coupling can either increase or decrease the effective magnetic moment, the magnitude of the variation being related to the spin (S) and orbital (L) quantum numbers. For an element with a shell more than half filled, the total moment quantum number J corresponds to $L - S$ and the effective moment is reduced by the spin–orbital coupling. This is the case in trivalent molybdenum ($4d^3$) for which $S = 3/2$, $L = 3$ and $J = 3/2$. Without any spin–orbit coupling the effective moment is equal to $2\sqrt{S(S+1)} = \sqrt{15} \approx 3.87\,\mu_B$. With a strong spin–orbit coupling [14] the effective moment is given by $g_J\sqrt{J(J+1)}$ with $g_J = [3J(J+1) + S(S+1) - L(L+1)]/2J(J+1)$. For a trivalent molybdenum $g_J = 0.4$ and the effective moment is equal to $0.2 \times \sqrt{15} \approx 0.77\,\mu_B$. This value is considerably reduced relatively to the effective moment calculated in the spin-only configuration. In Fig. 3, the measured effective moment evolution is compared to the theoretical ones for both spin-only and spin–orbital coupling of Mo^{3+}. For low Mo substitution, a classical spin-only behaviour appears to hold. But it seems that, above a certain Mo-doping rate corresponding to the stabilisation of the metallic phase in the whole thermal range, a strong spin–orbit coupling appears for trivalent molybdenum. Note that the effect would be similar if the spin–orbit coupling were to appear at the vanadium site instead of the molybdenum site (for the $3d^2$ configuration of V^{3+}: $S = 1$, $L = 3$, $J = 2$, and $g_J\sqrt{J(J+1)} = 2\sqrt{6}/3 \approx 1.63\,\mu_B$), or partially on both cation sites.

4. Magnetisation

The negative θ_p paramagnetic Curie temperatures (see Table 1) suggest the predominance of antiferromagnetic interactions in all samples. Nevertheless, recent EPR results [13] show the existence of a small ferromagnetic contribution in slightly oxidised samples. Attempts were made to detect such a contribution by performing magnetisation measurements as a function of applied field on several samples at various temperatures.

Two series of samples were considered, the first one kept in a glove box (10 ppm O_2) in between manipulations in air and measurements, and the second one annealed at 1000°C under dilute hydrogen (6% H_2, 94% N_2) just before measurements. EPR measurements [13] showed the presence of small amounts of V^{4+} in the first series (maximal value of 0.029% of V^{4+} per cation for $x = 20\%$) while no V^{4+} was detected in the second series.

Table 1
Molar Curie constants C_m, effective magnetic moments $M_{eff.}$ and paramagnetic Curie temperatures θ_P of $(V_{1-x}Mo_x)_{2-\delta}O_3$ for various doping rates

x% Mo	C_m exp. (emu)	$M_{eff.}$ exp. (μ_B)	θ_P (K)
0	1.67	2.58	−655
1	1.58	2.51	−730
2	1.64	2.53	−682
3	1.66	2.58	−605
4	1.69	2.60	−622
5	1.95	2.79	−627
7	1.78	2.67	−688
10	1.49	2.44	−558
20	1.29	2.27	−477

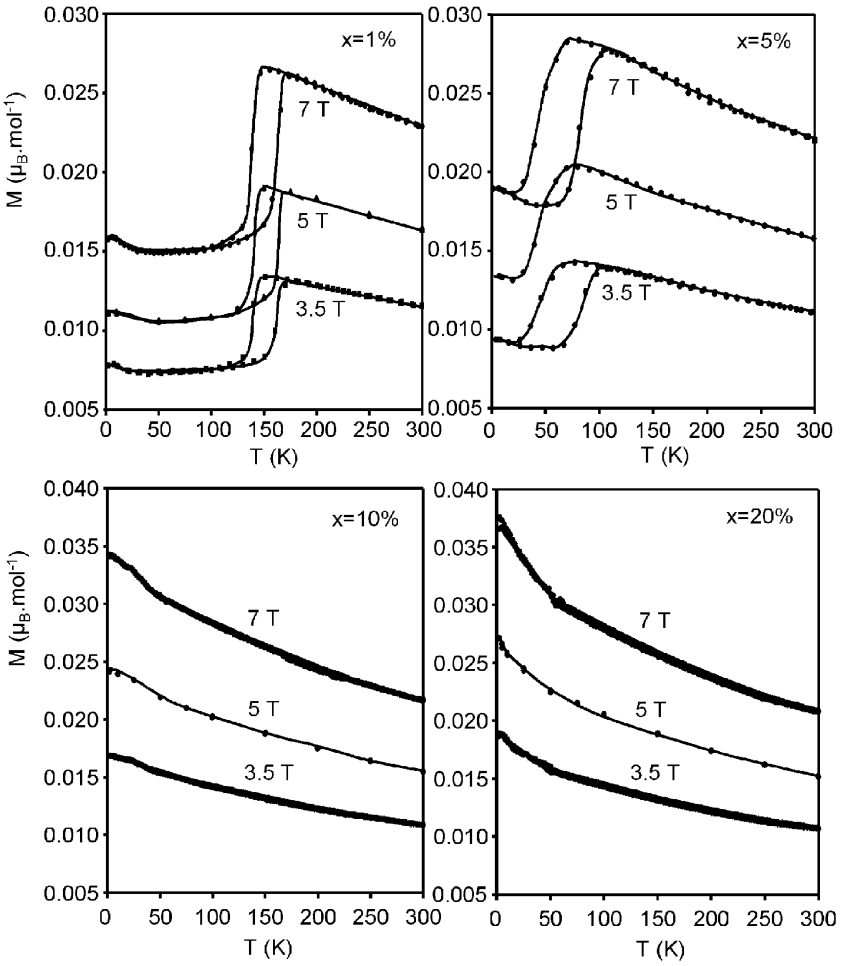

Fig. 4. Temperature dependence of the magnetisation of $(V_{1-x}Mo_x)_{2-\delta}O_3$ for $x = 1\%$, 5%, 10% and 20% under various fields (3.5, 5 and 7 T).

The magnetisation evolution as a function of temperature and magnetic field are shown in Fig. 4 for samples of the first series $x = 1\%$, 5%, 10% and 20%. The applied magnetic field has no influence on the width or temperature of the hysteresis cycle, when it exists.

At a given temperature, the magnetisation seems to evolve linearly as a function of field up to 7 T, irrespective of the temperature (see Fig. 5, left). However a closer examination at low field indicates the presence, at every temperature and for every oxidized samples (specially when $x = 20\%$), of a small curvature, suggesting the presence of a ferromagnetic contribution (see Fig. 5, right). Extrapolated to a zero field, the M_R remnant magnetisation corresponding to this contribution is very small. At room temperature it ranges from 5×10^{-5} to $5.1 \times 10^{-4}\,\mu_B$/mole depending on the sample (maximum value for $x = 20\%$). In those samples which exhibit a metal/insulator transition, the most important M_R are measured at room temperature, while in the samples with $x > 5\%$ it is at 2 K. However there is no evidence of a specific evolution of this ferromagnetic contribution with the Mo-doping rate.

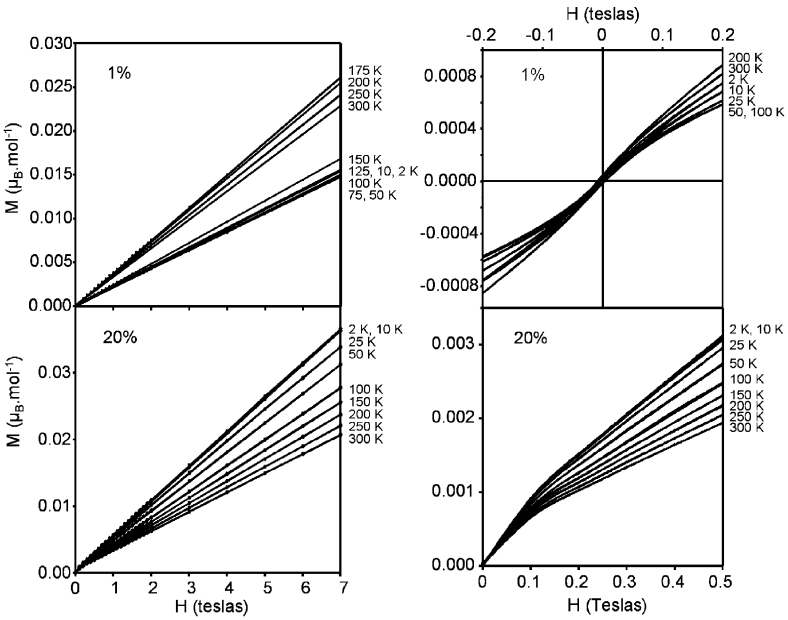

Fig. 5. Variation of the magnetisation of unannealed $(V_{1-x}Mo_x)_{2-\delta}O_3$ ($x = 1\%$ and 20%) as a function of the applied field at various temperatures. Left part: whole field range; right part: zoom on the small field region.

The observation of the most important curvature in the magnetisation at low field for the 20% Mo-doped sample (which is the most oxidised one, see above and Ref. [13]) tends to show that the ferromagnetic component is correlated to the oxidation of the samples, as evidenced by EPR measurements. It has been confirmed by magnetic measurements performed on the second series of samples, those which were reduced in dilute hydrogen and did not show any trace of vanadium oxidation in EPR measurements. In these samples including undoped V_2O_3, no curvature is observed in the magnetization, which evolves linearly with the applied field (see Fig. 6). Therefore from both magnetisation and EPR spectroscopy measurements, a clear correlation exists between weak ferromagnetism and oxidation.

There only is a small difference between the susceptibility characteristics of oxidized and stoichiometric undoped V_2O_3, as for instance molar Curie constants (1.69 and 1.67 emu, respectively) or paramagnetic temperatures (−624 and −643 K, respectively). The magnetisation curves of both samples are only slightly shifted with respect to each other without noticeable change in the transition temperature or hysteresis loop.

5. Magnetic structure

The thermodiffraction patterns of $(V_{0.97}Mo_{0.03})_{2-\delta}O_3$ recorded on D1B from room temperature down to 10 K are shown in Fig. 7. The most important magnetic reflections present in the monoclinic phase (space group I2/a) are indicated with an asterisk.

The extra reflections due to magnetic contribution can be indexed in the monoclinic cell but the I-lattice extinction conditions are not satisfied. The propagation vector of the magnetic structure, with components given in the conventional reciprocal basis of the group I2/a, is $\mathbf{k} = (0, 0, 1)$, which is an invariant vector: the group of the propagation vector is $G_{\mathbf{k}} = I2/a$. All magnetic reflections can be indexed using this propagation vector. The magnetic structure of $(V_{1-x}Mo_x)_{2-\delta}O_3$ in the

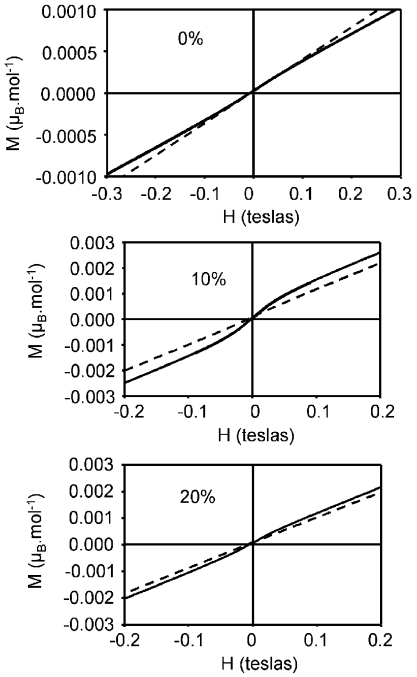

Fig. 6. Magnetisation curves at 300 K for $x = 0\%$, 5% and 20% oxidised (full lines) and reduced (dashed lines) samples of $(V_{1-x}Mo_x)_{2-\delta}O_3$.

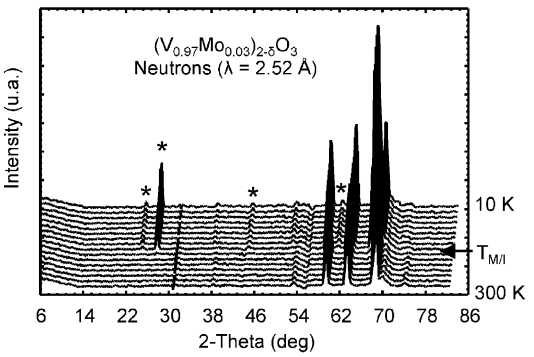

Fig. 7. Thermal evolution of the neutron diffraction pattern of $(V_{0.97}Mo_{0.03})_{2-\delta}O_3$ (main magnetic peaks are marked with a star).

monoclinic phase, determined using the Bertaut's method extended by Izyumov and co-workers [15], is similar to that of V_2O_3 reported earlier [16]. The complete symmetry analysis is summarised in Table 2, where we give the numbering of cations in a primitive cell (those not related by the centring translation), the irreducible representations of $G_{\mathbf{k}} = I2/a$ and the basis functions corresponding to the general position (V/Mo position) of magnetic atoms. The magnetic structure corresponds to the representation Γ_3, mode $F_xG_yF_z$. The Bertaut's notation here is misleading because the symbol F that was introduced for "ferromagnetic coupling" has nothing to do with ferromagnetism. The fact that $\mathbf{k} \neq (0,0,0)$ assures that there is no net magnetic moment. This magnetic structure corresponds to the I_P2'/a' magnetic space group according to the Opechowski and Guccione notation [17].

Fig. 8 shows the magnetic moment orientations in three independent planes of the monoclinic phase. These planes have been previously chosen (see [12]) in order to contain all symmetrically independent interactomic distances and angles (and therefore magnetic exchange paths) of the monoclinic phase. Plane π_h ($[10–2]_m$) corresponds to the hexagonal plane of the high-temperature rhombohedral phase, while planes π_1 $[0\,1\,0]_m$ and π_2 $[1\,1\,1]_m$, which are equivalent in the rhombohedral cell but not in the monoclinic one, show the pseudo-compact stacking of the π_h planes. The symmetry lift in the monoclinic cell relative to the rhombohedral one is clearly visible in the magnetic structure through the unequivalence of the magnetic arrangement in planes π_1 (ferromagnetic configuration) and π_2 (antiferromagnetic configuration).

The thermal evolution of the total magnetic moment is shown in Fig. 9 for each composition in the range $0 \leqslant x \leqslant 5\%$. The moments slightly decrease by about $0.10 \pm 0.04\,\mu_B$ whatever x from 10 K to the metal/insulator transition at which it abruptly disappears. Indeed the "natural" Néel temperature of the I phase would be much higher than the M/I transition temperature if this phase were stable. The analysis of each component of the magnetic moment along a crystallographic axis shows that the M_a component decreases while heating up. M_b is negligible and M_c remains practically constant with maybe a very small tendency to decrease before transition. There is no significant angle variation with the crystallographic axis ($<4^\circ$ whatever x).

Table 2
Irreducible representations of the propagation vector group for $\mathbf{k}=(0,0,1)$ in I2/a ($G_{\mathbf{k}}$ = I2/a) and basis functions for axial vectors bound to the Wyckoff site 8f
Matrices (characters) of the irreducible representations of $G_{\mathbf{k}}$ = I2/a

	1: (x,y,z)	2 $\{1/4,y,0\}$: $(-x+1/2,y,-z)$	$-1\{0,0,0\}$: $(-x,-y,-z)$	a $\{x,0,z\}$: $(x+1/2,-y,z)$
$\mathbf{\Gamma_1}$	1	1	1	1
$\mathbf{\Gamma_2}$	1	1	−1	−1
$\mathbf{\Gamma_3}$	1	−1	1	−1
$\mathbf{\Gamma_4}$	1	−1	−1	1

Basis functions of the irreducible representations of $G_{\mathbf{k}} = I2/a$ for axial vectors in the general position $8f$. The spins of the atoms related by the translation $\mathbf{t}(1/2,1/2,1/2)$, are obtained multiplying by the phase factor $\exp\{-2\pi i\mathbf{kt}\} = -1$

	C(1): (x,y,z)	C(2): $(-x+1/2,y,-z)$	C(3): $(-x,-y,-z)$	C(4): $(x+1/2,-y,z)$	Bertaut notation
$\mathbf{\Gamma_1}$	(1 0 0)	(−1 0 0)	(1 0 0)	(−1 0 0)	G_x
	(0 1 0)	(0 1 0)	(0 1 0)	(0 1 0)	F_y
	(0 0 1)	(0 0 −1)	(0 0 1)	(0 0 −1)	G_z
$\mathbf{\Gamma_2}$	(1 0 0)	(−1 0 0)	(−1 0 0)	(1 0 0)	A_x
	(0 1 0)	(0 1 0)	(0 −1 0)	(0 −1 0)	C_y
	(0 0 1)	(0 0 −1)	(0 0 −1)	(0 0 1)	A_z
$\mathbf{\Gamma_3}$	(1 0 0)	(1 0 0)	(1 0 0)	(1 0 0)	F_x
	(0 1 0)	(0 −1 0)	(0 1 0)	(0 −1 0)	G_y
	(0 0 1)	(0 0 1)	(0 0 1)	(0 0 1)	F_z
$\mathbf{\Gamma_4}$	(1 0 0)	(1 0 0)	(−1 0 0)	(−1 0 0)	C_x
	(0 1 0)	(0 −1 0)	(0 −1 0)	(0 1 0)	A_y
	(0 0 1)	(0 0 1)	(0 0 −1)	(0 0 −1)	C_z

All representations are one-dimensional. The magnetic atoms, $C(i)$, are numbered according to the ordering of symmetry operators, the atoms related by the centring translation.
Symmetry elements are labelled by the conventional crystallographic symbol and their localisation is given between curly brackets. The global magnetic representation Γ_M, direct product of the axial $V(3\times3)$ and permutation $P(4\times4)$ representations, contains three times each irreducible representation: $\Gamma_M = 3\Gamma_1 \oplus 3\Gamma_2 \oplus 3\Gamma_3 \oplus 3\Gamma_4$, so the total number of basis function is three for each representation.

For 10% and 20% Mo substitutions the rhombohedral phase remains metallic and paramagnetic all over the studied thermal range. The low temperature neutron diffraction patterns do not show any other reflections, nor any significant increase of the nuclear reflection intensities for $x =$ 10% (see Fig. 10) and $x = 20\%$. Therefore in Mo-doped V_2O_3 there is no magnetic order even down to 1.5 K in the samples that do not exhibit any metal/insulator transition.

The effect of Mo-doping at low doping rate on the magnetic structure of V_2O_3 has been studied at 10 K (see Fig. 11 for two examples of observed and calculated neutron diffraction patterns). The evolution of the magnetic moment components as a function of doping at this temperature is presented in Fig. 12. This figure also shows the angle variation between the M_{tot} total magnetic moment and the c_h hexagonal axis (right).

At 10 K the M_a magnetic moment component, along the a_m monoclinic axis, tends to slightly increase with Mo-doping rate while the M_c component, along the c_m axis, decreases. As the moment component along the b_m axis is always close to zero after refinement, with an error bar usually superior to the value of the moment along that direction, it is neglected. The average value of the total magnetic moment ($M_{total} = 1.15(2)\,\mu_B$),

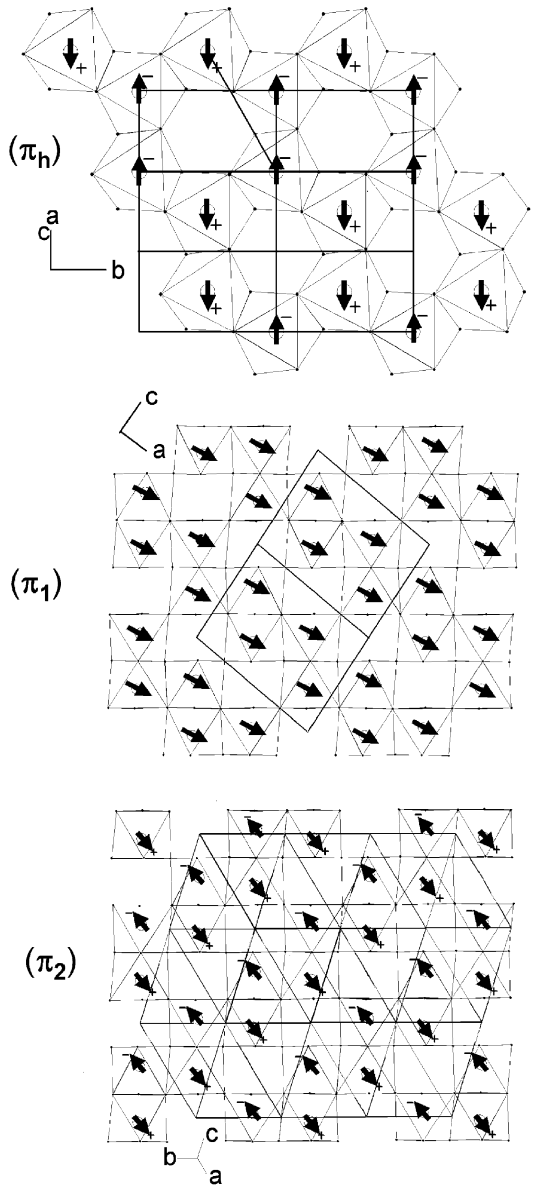

Fig. 8. Magnetic moments configuration of $(V_{1-x}Mo_x)_{2-\delta}O_3$ ($x \leqslant 5\%$) within the three representative independent planes π_h, π_1 and π_2 (see text).

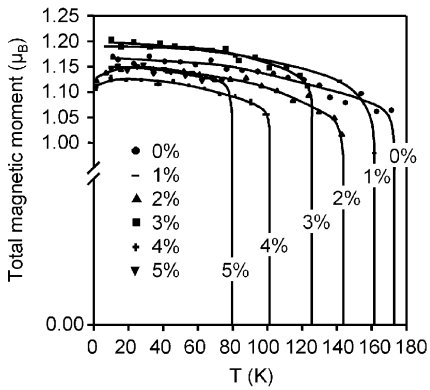

Fig. 9. Thermal variation of the low temperature total magnetic moment of $(V_{1-x}Mo_x)_{2-\delta}O_3$ for $x = 0\%$, 1%, 2%, 3%, 4% and 5%.

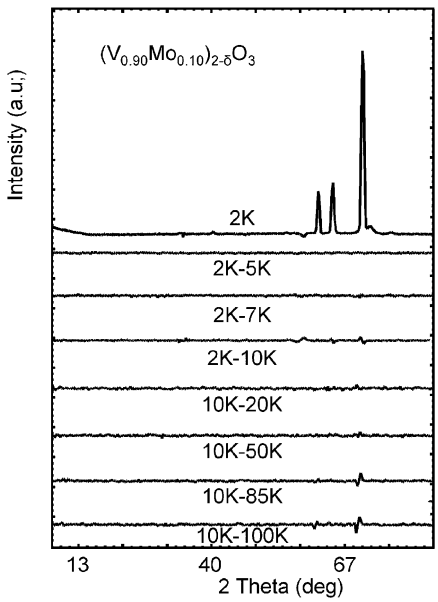

Fig. 10. Neutron diffraction pattern of $(V_{0.90}Mo_{0.10})_{2-\delta}O_3$ at 2 K, and difference patterns showing the absence of any magnetic contribution.

still very small compared to the theoretical $2\,\mu_B$ for $S = 1$, tends to decrease while the Mo-doping rate increases, in contrast with the effective moment in the paramagnetic phase which increases (see above).

The magnetic moments get closer to the direction of the a_m axis in the monoclinic cell, and to that of the c_h axis in the hexagonal one, with an angle which decreases of $13 \pm 5^\circ$ when x varies from 0% to 5% (see Fig. 12).

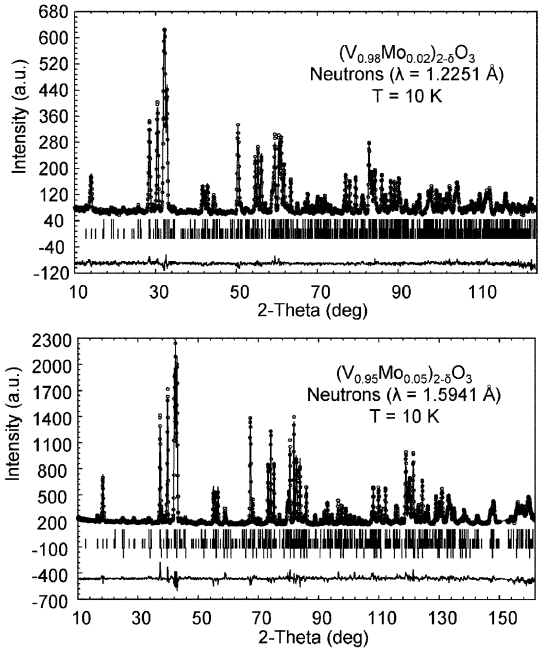

Fig. 11. Observed (dots), calculated (lines) and difference (below) neutron diffraction patterns of $(V_{1-x}Mo_x)_{2-\delta}O_3$ ($x = 2\%$ and 5%) at 10 K. Note, for $x = 5\%$, the presence of diffraction peaks of the high-temperature non-magnetic rhombohedral phase (third row in the reflection lines). Reliability factors:

- for $(VO_{.95}MO_{0.02})_{2-\delta}O_3$: $R_p = 0.100$, $R_{wp} = 0.084$, $R_{exp} = 0.067$, $\chi^2 = 1.560$, $R_B = 0.048$, $R_F = 0.034$ and $R_{Mag.} = 0.145$
- for $(VO_{.95}MO_{0.05})_{2-\delta}O_3$: $R_p = 0.142$, $R_{wp} = 0.132$, $R_{exp} = 0.062$, $\chi^2 = 4.530$, $R_B = 0.089$, $R_F = 0.075$ ($R_B = 0.061$, $R_F = 0.055$) and $R_{Mag.} = 0.140$.

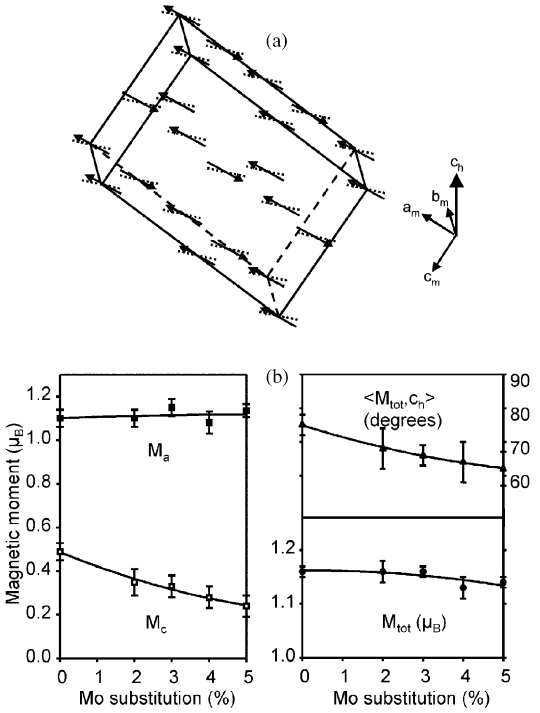

Fig. 12. (a) Magnetic structure of $(V_{1-x}Mo_x)_{2-\delta}O_3$ for $x = 0\%$ (dotted) and $x = 5\%$ (arrows). (b) Evolution with x of the magnetic moment components (left), and of the total moment and angle with the c pseudo-hexagonal axis (right) in $(V_{1-x}Mo_x)_{2-\delta}O_3$ at 10 K.

6. Summary and conclusions

The magnetic properties of the $(V_{1-x}Mo_x)_{2-\delta}O_3$ family have been characterised from a series of magnetic susceptibility, magnetisation, and neutron diffraction measurements below room temperature.

The susceptibility measurements show an antiferromagnetic transition simultaneous to the structural and electrical transitions. In the paramagnetic state of the metallic phase, susceptibility follows a Curie–Weiss law with a largely negative paramagnetic Curie temperature, indicating predominant antiferromagnetic couplings. The effective moment deduced from the Curie constant shows a peculiar variation as a function of doping, reaching a maximum value at $x = 5\%$. For upper values of x, the effective moment decrease could be explained by a spin–orbital coupling between cations, but this point still has to be confirmed by other techniques.

Consistently with previous EPR results, magnetisation measurements let appear a weak ferromagnetic component (around $10^{-4}\,\mu_B$/mole) clearly correlated to partial oxidation of the samples in air. The origin of this component, either intrinsic to oxidized samples or resulting from a very partial decomposition due to oxidation, is still unclear and would deserve a specific investigation. It seems likely that, whatever the exact nature of the oxidized phase, oxidation essentially takes place at the surface of the particles. An in-depth study of this interesting behaviour as a function of oxidation and

other parameters such as grain size would be necessary for a better understanding of the phenomenon.

Neutron diffraction shows that the metal/insulator transition, when it exists (for $x \leqslant 5\%$), is accompanied by an abrupt magnetic ordering of the same type as that observed for V_2O_3. A similar magnetic moment reduction at saturation is observed, certainly due to a partial electronic delocalisation [18]. The magnitude of the magnetic moment at saturation changes only weakly as a function of the doping rate. However the magnetic moment direction gets closer to the c_h pseudo-hexagonal axis when the Mo-doping rate increases. For higher values of x the metallic phase is stable over the whole thermal range. On a magnetic point of view, an interesting comparison can be made with isotypic Ti-doped V_2O_3 in which, above a certain doping rate, a new magnetic phase (AF with a spin density wave) orders around 10 K within the metallic state [19,20]. At reverse in highly Mo-doped V_2O_3 no magnetic order is observed down to 1.5 K, the compounds remaining in a paramagnetic state.

References

[1] M. Foex, C. R. Acad. Sci. 223 (1946) 1126.
[2] M. Foex, C. R. Acad. Sci. 229 (1949) 880.
[3] N.F. Mott, Proc. Phys. Soc. A 62 (1949) 416.
[4] A. Menth, J.P. Remeika, Phys. Rev. B 2 (1970) 3756.
[5] M. Yethiraj, J. Solid State Chem. 88 (1990) 53.
[6] R.M. Moon, J. Appl. Phys. 41 (1970) 883.
[7] R.M. Moon, Phys. Rev. Lett. 25 (1970) 527.
[8] L. Paolasini, C. Vettier, F. de Bergevin, F. Yakhou, D. Mannix, A. Stunault, W. Neubeck, M. Altarelli, M. Fabrizio, P.A. Metcalf, J.M. Honig, Phys. Rev. Lett. 82 (1999) 4719.
[9] C. Tenailleau, Ph.D. Thesis, University of Le Mans, France, 2001.
[10] P. Lacorre, C. Tenailleau, Solid State Sci. 4 (2002) 217.
[11] C. Tenailleau, E. Suard, J. Rodriguez-Carvajal, M.-P. Crosnier-Lopez, P. Lacorre, Chem. Mater. 14 (2002) 3569.
[12] C. Tenailleau, E. Suard, J. Rodriguez-Carvajal, A. Gibaud, P. Lacorre, J. Solid State Chem. 174 (2003) 331.
[13] C. Tenailleau, A.H. Kassiba, P. Lacorre, J. Phys. Chem. Solids, submitted for publication.
[14] D. Craik, Magnetism: Principles and Applications, Wiley, New York, 1995.
[15] E.F. Bertaut, In: G.T. Rado, H. Suhl, (Eds.), Magnetism, Vol. III, Academic Press, New York, 1963, p. 149. See also: Y.A. Izyumov, V.E. Naish, R.P. Ozerov, Neutron Diffraction of Magnetic Materials, Consultants Bureau, Plenum, New York, 1991.
[16] W.B. Yelon, S.A. Werner, S. Shivashankar, J.M. Honig, Phys. Rev. B 24 (1981) 1818.
[17] W. Opechowski, R. Guccione, in: G.T. Rado, H. Suhl (Eds.), Magnetism, Vol. IIA, Academic Press, New York, 1965, p. 105.
[18] C. Castellani, C.R. Natoli, J. Ranninger, Phys. Rev. B 18 (1978) 4945.
[19] J. Dumas, C. Schlenker, J. Magn. Mater. 7 (1978) 252.
[20] Y. Ueda, K. Kosuge, S. Kachi, T. Takada, J. Phys. C2 (1979) 275 (Paris).